Eur. Phys. J. C (2025) 85:971
https://doi.org/10.1140/epjc/s10052-025-14709-6

THE EUROPEAN PHYSICAL JOURNAL C

Regular Article - Theoretical Physics

Stability and topological thermodynamics of black holes through modified entropy

Shamaila Rani[1,2,a], **Hifza Riaz**[2,b], **Usman Zafar**[3,c], **Abdul Jawad**[2,1,d], **N. Myrzakulov**[4,e], **Sanjar Shaymatov**[5,6,7,8,f]

[1] Institute for Theoretical Physics and Cosmology, Zhejiang University of Technology, Hangzhou 310023, China
[2] Department of Mathematics, COMSATS University Islamabad, Lahore-Campus, Lahore 54000, Pakistan
[3] Faculty of Symbiotic Systems Science, Fukushima University, Fukushima 960-1296, Japan
[4] L. N. Gumilyov Eurasian National University, 010008 Astana, Kazakhstan
[5] Institute of Fundamental and Applied Research, National Research University TIIAME, Kori Niyoziy 39, 100000 Tashkent, Uzbekistan
[6] University of Tashkent for Applied Sciences, Str. Gavhar 1, 100149 Tashkent, Uzbekistan
[7] Western Caspian University, AZ1001 Baku, Azerbaijan
[8] Tashkent State Technical University, 100095 Tashkent, Uzbekistan

Received: 8 June 2025 / Accepted: 30 August 2025

Abstract We explore higher-dimensional black holes (BHs) using the Sharma–Mittal entropy, a widely employed measure in BH thermodynamics due to the non-extensive nature of BHs. We compute different thermodynamic quantities like temperature, heat capacity, and Gibbs free energy to study the stability of higher-dimensional BHs in Einstein–Gauss–Bonnet gravity (EGBG). We explicitly analyze the behavior for different horizon topologies (parameterized by k) in EGBG and observe that these BH exhibit both local and global instability. Additionally, we study the sparsity of Hawking radiation, noting that the sparsity parameter tends to zero as the horizon radius increases. It is also observed that emission of energy radiates most rapidly for larger BHs, which is consistent with physical observations. Furthermore, to support our analysis, we choose thermodynamical topology methods (specifically, the temperature and on-shell Gibbs free energy) to observe the stability of the aforementioned BH solutions. It is found that the total topological charge obtained from the free energy method leads to $+1$ for specific values of k, which also gives the confirmation of the stability of these BH solutions in EGBG for a specific choice of other constant parameters.

[a] e-mail: drshamailarani@cuilahore.edu.pk
[b] e-mail: hifzariaz016@gmail.com
[c] e-mails: zafarusman494@gmail.com; s2471001@ipc.fukushima-u.ac.jp
[d] e-mail: abduljawad@cuilahore.edu.pk (corresponding author)
[e] e-mail: nmyrzakulov@gmail.com
[f] e-mail: sanjar@astrin.uz

1 Introduction

The theory of general relativity (GR), developed by Einstein, is acclaimed as one of the most successful scientific theories owing to strong experimental observation. GR predicted the existence of black holes (BHs), which continue to be a compelling subject of study, bridging the gap between classical GR and quantum gravity [1–5]. A BH is a fascinating cosmic phenomenon where nothing, not even light, can escape its intense gravitational pull. Gravitational collapse in massive stars leads to the formation of BHs, where spacetime becomes intensely dense, and it challenges conventional physics. BHs evolved from theoretical concepts to observable realities towards the end of the 20th century. The discovery of quasars in the 1960 s provided strong evidence for supermassive BHs at galactic centers, and in 2019, the Event Horizon Telescope captured the first image of a BH's shadow, confirming predictions from GR [6]. Recent research has expanded to include thermodynamics and quantum mechanics, with studies on higher-dimensional BHs helping scientists better understand these complex cosmic entities and their influence on the universe [7–9].

BH thermodynamics has become a pivotal area of research, forging connections between classical general relativity and quantum theories of gravity. Understanding quantum gravity heavily relies on BH thermodynamics, which associates general relativity, quantum field theory, and statistical mechanics [10]. Bekenstein and Hawking suggested that BHs share thermodynamic attributes such as entropy and temperature

Published online: 11 September 2025

with ordinary systems [3,4]. A key motivation for exploring BH thermodynamics is to gain insight into the statistical mechanics of BHs, where entropy is linked to numerous microstates [11–14]. This may profoundly shape our comprehension of quantum gravity, guiding the establishment of the holographic principle [15–17]. Another important goal is to study the possible phase transitions and critical behavior that may arise in BH systems, including the Hawking-Page transition linking a Schwarzschild BH to thermal radiation in anti-de Sitter (AdS) space [11,13–15]. Many fascinating and challenging topics arise in BH thermodynamics, such as understanding the source and properties of BH entropy, addressing the information paradox, incorporating quantum modifications to classical laws, exploring pressure and volume effects in extended phase space, and analyzing the thermodynamics of many BHs [18–25]. The thermodynamic behavior in AdS spacetime of BHs includes Hawking-Page transitions where thermal radiation changes into stable large BHs, similar to the phase change between liquid and gas in van der Waals systems (Extensive research has been conducted to analyze the stability and $P - V$ criticality of the various BHs for details, check Refs. [26–34]).

Furthermore, the Bekenstein–Hawking entropy formula ($S = A/4G$) assumes BHs behave like simple, additive systems, but this doesn't fully hold due to quantum gravity effects and entangled particle interactions near their boundaries [35–37]. These complexities make BHs non-extensive, meaning their entropy doesn't scale linearly with size like ordinary matter. To address this, scientists explore alternative entropy frameworks – such as Tsallis, Rényi, and Sharma–Mittal models – to better explain how BHs store and manage information (for more detailed analysis regarding the generalized entropies and their impact on BH thermodynamics, see Refs. [37–40]). Sharma–Mittal entropy serves as a generalized entropy model that combines characteristics of Rényi and Tsallis entropy, facilitating the analysis of systems exhibiting irregular thermodynamic behaviors, similar to BHs [36]. Higher-dimensional BHs have been developed by including the Gauss–Bonnet (GB) correction in the action, which is known as EGBG in the presence of AdS (Anti-de Sitter) [41]. Various thermodynamic features such as phase transitions of the particles, stability, and topological thermodynamics have been studied with the GB corrections in the action. These analyses suggest that incorporating the GB term gives physically meaningful results under the aforementioned conditions.

Apart from classical thermodynamic aspects, BH thermodynamics has been investigated using thermodynamic geometry and thermodynamic topology, which provide crucial insights into stability and critical phenomena. The growing interest in the connection between topology and BH thermodynamics has led researchers to adopt topological techniques to better understand the stability, behavior, and phase transitions of BH systems [42–45]. For instance, topological defects, winding numbers, and topological charges can be utilized to categorize both local and global characteristics of the BH thermodynamic parameter space [42,43]. Additionally, the Brouwer degree, a topological invariant, can be employed to capture the fundamental properties of critical points in BH thermodynamics. By applying topological approaches like Duan's topological current theory, this framework enables the analysis of BH critical points and phase structures in an invariant fashion [42,43]. From a thermodynamic standpoint, topology serves as a tool to highlight the similarities and differences between different types of BHs (thermodynamic topology has been studied for numerous BH frameworks [46–55]).

Hawking radiation does not exhibit a continuous spectrum like that of a classical blackbody; rather, it appears as widely separated quanta, a feature known as radiation sparsity. Even when the Hawking temperature remains fixed, a BH does not radiate in a continuous manner like classical blackbodies, but rather in quantized emissions [56]. This sparsity of Hawking radiation plays an important role in its detectability and quantum information in the context of Hawking radiation. It was shown in Ref. [57] that neither the spin of the particle nor the dimensionality of spacetime alters the sparsity parameter, affirming that the discreteness in Hawking radiation is a general phenomenon. The outline of this paper is as follows. In Sect. 2, we briefly discuss the BH solution in Einstein–Gauss–Bonnet gravity and also describe the Sharma–Mittal entropy in Einstein–Gauss–Bonnet gravity. In Sect. 3, we study the thermodynamic quantities of this BH solution by using Sharma–Mittal entropy. In Sect. 4, we discuss the sparsity of Hawking radiation and emission of energy via Sharma–Mittal entropy. In Sect. 5, we discuss the thermodynamic topology of BHs via Sharma–Mittal entropy using temperature and Gibbs free energy (GFE) methods, determining the topological charge (winding number) for stability analysis. In Sect. 6, finally, we present our conclusion.

2 Black holes in Einstein–Gauss–Bonnet gravity

In this section, we describe the solution of the BH in EGBG and also corresponding thermodynamic quantities by using the framework of Sharma–Mittal entropy. The five-dimensional action of the Einstein-Maxwell GBG is given by [58]

$$\mathcal{S} = \frac{1}{16\pi}\int \mathrm{d}^5x\sqrt{-g}\big[R - 2\Lambda + \frac{\alpha}{2}(R_{\mu\nu\rho\alpha}R^{\mu\nu\rho\alpha} - 4R_{\mu\nu}R^{\mu\nu} + R^2) - 4\pi F_{\mu\nu}F^{\mu\nu}\big] + \mathcal{S}_b, \tag{2.1}$$

where $\sqrt{-g}$ represents the determinant of the metric, R is the Ricci scalar and $\Lambda = -\frac{6}{\ell^2}$ is the cosmological constant.

Furthermore, α denotes the GB coupling coefficient with AdS spacetime, $R_{\mu\nu\rho\alpha}$ is the Riemann curvature scalar, R^2 is the Ricci squared scalar, $F^{\mu\nu}$ is the Maxwell field strength and $\mathcal{S}_b$ is the boundary term that may appear due to the integration by parts. The metric for an AdS BH in EGBG is given in the following expression

$$ds^2 = -f(r)dt^2 + f^{-1}(r)dr^2 + r^2 d\Omega_3^2 \tag{2.2}$$

where $d\Omega_3^2 = d\theta^2 + \sin^2\theta d\phi^2 + \cos^2\theta d\psi^2$ denotes the line element for unit 3-sphere and $f(r)$ represent the metric function that depends on the mass of the BH, charge, and GB coupling constant, and nonlinear electrodynamics (NED) parameters. The general solution of the BH is obtained by solving the equations of motion that follow from Eq. (2.1). In the present scenario, the metric function turns out to be

$$f(r) = k + \frac{r^2}{2\alpha}\left(1 - \sqrt{1 + \frac{32\alpha M}{3\pi r^4} - \frac{16\alpha Q^2}{3\pi^2 r^6} - \frac{4\alpha}{l^2}}\right), \tag{2.3}$$

Later on, we use $f(r) = f(r_+)$, which defines the spacetime properties in the area near the BH horizon. Here, Q and M are the integration constants corresponding to the BH's charge and mass, respectively. The parameter l is called the AdS radius and is related to the cosmological constant. The solution $f(r_+) = 0$ defines the radius of the event horizon, which is crucial to comprehending the thermodynamic quantities such as temperature and entropy. Moreover, k defines the shape of the horizon, whether spherical, planar, or hyperbolic. For example, if the horizon varies with the parameter k,

- becomes a positively curved 3-sphere for $k = 1$,
- a flat Euclidean space for $k = 0$,
- a hyperbolic space with negative curvature when $k = -1$.

Consequently, different k values result in topological BHs whose thermodynamic characteristics and stability are notably influenced by the underlying horizon topology. It is observed that the GB term interacts with k and it plays a key role in analyzing the effects of curvature modifications in BH dynamics. Also, GB coefficient (α) determines the role of higher-order curvature corrections. At smaller α, the system approximates standard Einstein gravity, while a large α produces significant variations.

3 Thermodynamic quantities by Sharma–Mittal entropy

In this section, we obtain some thermodynamic quantities like mass, temperature, heat capacity, and gibbs free energy. Before delving into studying thermodynamics, we first compute the mass of the BH, which can be obtained by using the expression for M from Eq. (2.3) into $f(r)|_{r=r_+} = 0$, which yields

$$M = \frac{\pi}{8}\left(3kr_+^2 + 4\pi P r_+^4 + 3\alpha k^2\right) + \frac{Q^2}{2\pi r_+^2}, \tag{3.1}$$

This equation explains the mass M associated with a charged AdS BH in the GB framework in five-dimensional spacetime. It integrates key elements: The first term indicates the addition of the geometry of the BH horizon, where k signifies the geometry of the event horizon, such as spherical $k = 1$, planar $k = 0$, or hyperbolic $k = -1$. The second term relates to the BH mass in relation to the thermodynamic pressure P, focusing on the expanded thermodynamic approach, where Λ is interpreted as a dynamic thermodynamic pressure and can be defined as

$$P = \frac{3}{4\pi\ell^2}. \tag{3.2}$$

The third term is the adjustment resulting from the GB contribution, focusing on the impact of higher-dimensional curvature factors in adjusting the BH's energetic structure. The last component signifies the electrical influence contributed by charge Q.

The Bekenstein–Hawking entropy plays a central in BH thermodynamics, highlighting that BH entropy is directly linked to the area of its event horizon. It establishes a connection between quantum mechanics and general relativity by considering BHs as thermodynamic phenomena. This framework established the foundation for Hawking radiation, demonstrating that BHs emit thermal energy, prompting significant discussions of the BH information paradox [3,59,60]. However, in classical thermodynamics, entropy is associated with the volume of a system, whereas for BHs, it scales with the surface area of the event horizon, and this area law relation of BH can be broken down in the presence of higher-dimensional gravity theories like GBG. Hence, in order to analyze the thermodynamic behavior of this BH, we consider the Sharma–Mittal entropy, a generalized combination of the Tsallis and the Rènyi entropies (for more details regarding generalized entropies and their application in BH thermodynamics, see Refs. [38,61–68]). Moreover, the Sharma–Mittal entropy introduces a framework that generalizes the Rényi and Tsalli entropies with two parameters. It is particularly beneficial in systems that require a flexible approach to handling probability sensitivity. It is useful in BH thermodynamics by clarifying generalized entropy-area relationships and the stability of the system under varying statistical frameworks [69–71]. By adopting the mathematical formulation given in the literature [72,73]. Following

this, we define

$$S_{\rm SM} = \frac{1}{R}\left(\left(1+\delta S_{\rm T}\right)^{\frac{R}{\delta}} - 1\right), \tag{3.3}$$

where R, δ are the dimensionless free parameters which are obtained by comparing with the observational data as mentioned in Refs. [37,69,74]. The parameter R acts as a deformation parameter akin to Rènyi entropy and δ governs the non-additivity inherited from Tsallis entropy Refs. [36,37,69,74]. In BH thermodynamics, large values of δ enhance the non-extensive impacts, which leads to the negative behavior of heat capacity and increased instability in small BHs, while a higher value of R leads to smoothing the thermodynamic quantities like temperature and heat capacity. These two parameters of Sharma–Mittal entropy distinctly govern the non-extensive thermodynamics characteristics of BHS [62,66]. Together, they significantly modify the behavior of heat capacity and GFE, which impacts both local and global thermodynamic stability of BHs. In addition, $S_{\rm T}$ is entropy associated with the GB entropy. The entropy of BHs in higher dimensions under GBG is determined through the following formula.

$$S_{\rm T} = \frac{\pi^2 r_+^3}{2}\left(1+\frac{6k\alpha}{r_+^2}\right), \tag{3.4}$$

By incorporating the above entropy in the Sharma–Mittal expression, one can get the final expression of the Sharma–Mittal entropy, which turns out to be

$$S_{\rm SM} = \frac{-1+\left(1+\frac{\pi^2 r_+}{2}\left(r_+^2+6k\alpha\right)\delta\right)^{\frac{R}{\delta}}}{R}. \tag{3.5}$$

Sharma–Mittal entropy provides a generic framework to examine the higher-dimensional BHs under the Guass–Bonnet gravity as compared to Tsallis and Rènyi entropy models. In BH physics, Tsallis and Rènyi entropy frameworks are often utilized to study non-extensive thermodynamic behavior, particularly in contexts where higher curvature or quantum gravity terms cause the ambiguity in the Bekenstein–Hawking's area law. However, Sharma–Mittal entropy provides a generic framework that incorporates both entropy models for example, we can retrieve Rènyi entropy when $R \to 0$ and Tsallis entropy when $R \to \delta$ [36,37]. By introducing two parameters, this framework permits a more flexible approach to departures from additivity and extensivity, specifically in the presence of higher-order curvature effects associated with Gauss–Bonnet gravity. The Sharma–Mittal entropy framework is more suitable to characterize the non-trivial modification in BH's horizon geometry and thermodynamic volume by such corrections. Due to its interpolating relation between the Rènyi and Tsallis entropy frameworks, Sharma–Mittal entropy provides a unique approach to study intricate phase transitions and critical phenomena, which is crucial to investigating the topological and thermodynamic aspects such as winding number, topological charge, sparsity of Hawking radiation, and energy emission rate. In the context of Einstein–Gauss–Bonnet gravity, Sharma–Mittal entropy provides a more comprehensive and dynamically effective approach to examining thermodynamic behavior, surpassing other entropy models that may fail to integrate both non-extensive aspects.

3.1 Temperature

Moreover, it is straightforward to obtain the conjugate temperature related to the Sharma–Mittal entropy by employing the given relation

$$T = \left(\frac{\partial M}{\partial S_{\rm SM}}\right)_{P,Q,\alpha}. \tag{3.6}$$

This equation is obtained from the principles of the first law of BH thermodynamics as expanded in the modified paper to include further parameters such as pressure (P) and the GB coupling parameter (α). In this context, M is recognized as the enthalpy within the BH model. The equation associates the thermodynamic temperature (T) with the differential of enthalpy (M) in terms of entropy $(S_{\rm SM})$ with fixed P, Q and α.

According to the first law of BH thermodynamics, the change in mass of a BH is related to its physical characteristics, like angular momentum, charge, and horizon area. This law is significant for studying the behavior of BHs and has been a core concept in research, particularly in the context of modified gravity theories and BH dynamics [75,76]. The expression for the first law of BH thermodynamics is given as follows

$$\mathrm{d}M = T\mathrm{d}S_{\rm SM} + V\mathrm{d}P + \phi\mathrm{d}Q + A\mathrm{d}\alpha, \tag{3.7}$$

$$T = \left(\frac{\partial M}{\partial S_{\rm SM}}\right)_{P,Q,\alpha}, V = \left(\frac{\partial M}{\partial P}\right)_{S_{\rm SM},Q,\alpha},$$
$$A = \left(\frac{\partial M}{\partial \alpha}\right)_{S_{\rm SM},Q,P}, \phi = \left(\frac{\partial M}{\partial Q}\right)_{S_{\rm SM},P,\alpha}, \tag{3.8}$$

where $S_{\rm SM}$, Q, ϕ, and P are thermodynamic variables for the function. However, T, ϕ, and V are variables and conjugate to $S_{\rm SM}$, Q, and P, respectively. However, the temperature can be calculated as

$$T = \frac{2^{-2+\frac{R}{\delta}} r_+ \left(2+\pi^2 r_+\left(r_+^2+6k\alpha\right)\delta\right)^{1-\frac{R}{\delta}}\left(3k+8P\pi r_+^2-4\phi^2\right)}{3\pi\left(r_+^2+2k\alpha\right)}. \tag{3.9}$$

This equation describes how the temperature varies with the horizon radius (r_+), the pressure (P), the electric potential (ϕ), and the GB coupling (α). Figure 1 shows the behavior of the conjugate temperature corresponding to the Sharma–Mittal entropy as a function of the horizon radius for dif-

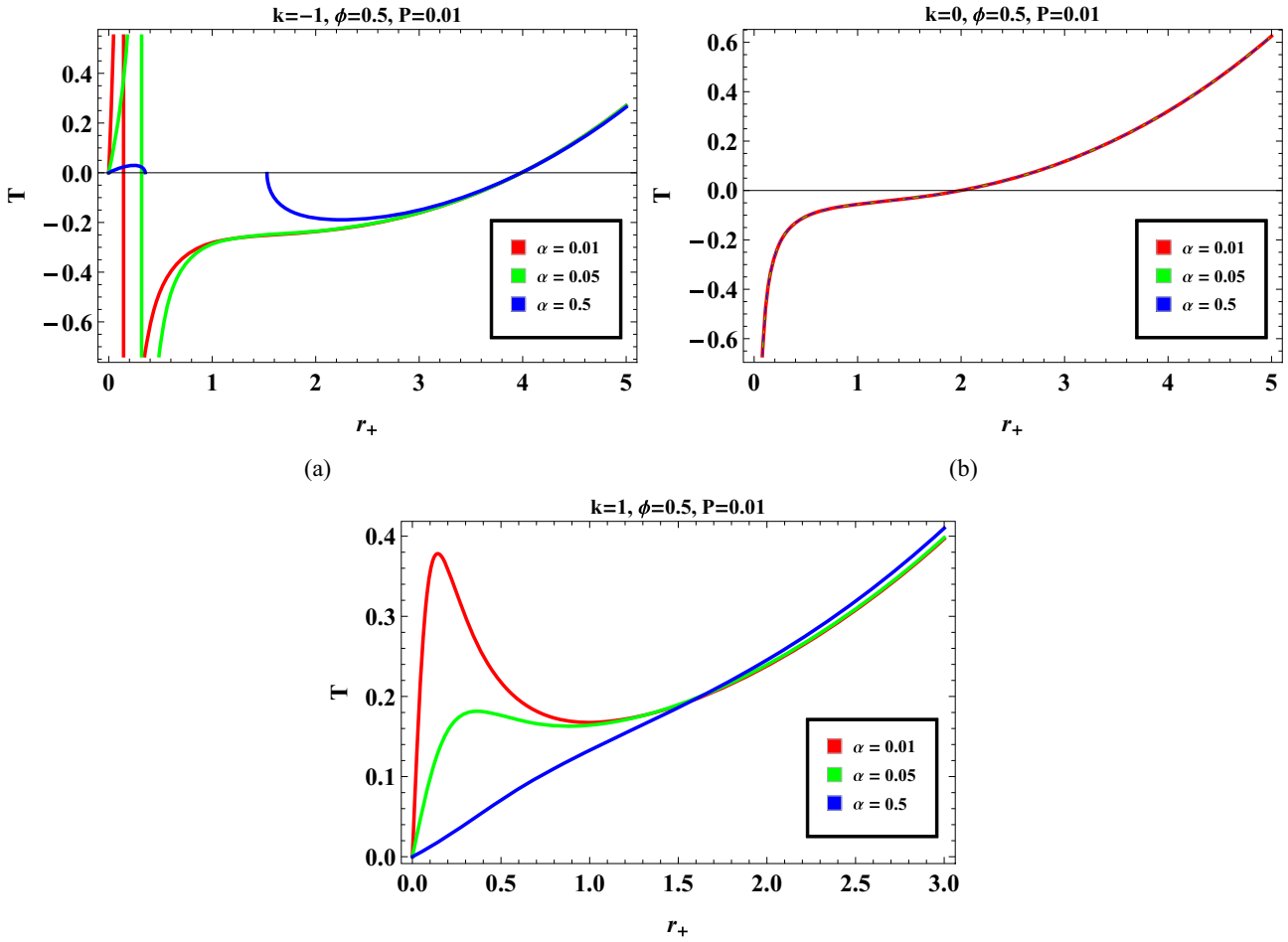

Fig. 1 Plots of thermodynamic temperature versus horizon radius for BH solutions with $k = -1$ (**a**), $k = 0$ (**b**) and $k = 1$ (**c**). The red, green, and blue curves correspond to three values of $\alpha = 0.01,\ 0.05,\ 0.5$, respectively

ferent values of α. We obtain this behavior by fixing the values of $\phi = 0.5,\ P = 0.01,\ \alpha = 0.01,\ 0.05,\ 0.5$ and $k = -1,\ 0, 1$ in Fig. 1a–c respectively. We observe that in Fig. 1a for $k = -1$, temperature is negative initially for smaller values of the horizon radius and its behavior become positive as the horizon radius increases. In Fig. 1b for $k = 0$, the behavior of temperature shows increasing behavior with negative behavior for smaller values of the horizon radius and after some interval of the horizon radius the behavior of the temperature grows as the horizon radius increases. Notably, it is observed that that for $k = 1$ temperature behavior is positive for all the values of the horizon radius. Furthermore, it is observed that the phase transition is more significant at lower values of α and horizon radius, whereas increasing α leads to a smoother curve, indicating a stable BH. They highlight the temperature curve associated with different values of k in Fig. 1a–c. Phase transitions occur at small values of the horizon radius in Fig. 1a, b.

3.2 Heat capacity

In BH thermodynamics, the energy needed to alter the BH's temperature is referred to as heat or thermal capacity, which is a crucial and measurable physical quantity. One can determine whether a BH is stable or unstable based on the sign, where a positive value indicates stability, and a negative value indicates instability. There are two different types of heat capacity: C_V, which assesses the specific heat at constant volume, and C_P, which determines the specific heat at constant pressure. It is observed that Eq. (3.1) serves as the basis for determining the heat capacity to analyze local stability, therefore, the specific heat at constant pressure and electric potential can be computed by employing the following equation.

$$C_\phi = T\left(\frac{\partial S_{\rm SM}}{\partial T}\right)_{P,\phi}. \tag{3.10}$$

This equation determines the heat capacity C_ϕ of a BH in a situation where the electric field potential ϕ and the pressure P remain fixed. Heat capacity is an important thermodynamic property utilized to evaluate the local stability of the BH. Applying the equation of entropy 3.5, one can obtain the following result

$$\begin{aligned} C_\phi = &\left(3\pi^2 r_+(r_+^2+2k\alpha)^2\left(1+\frac{1}{2}\pi^2 r_+(r_+^2+6k\alpha)\delta\right)^{\frac{R}{\delta}}\right.\\ &(3k+8P\pi r_+^2-4\phi^2)\Big)\Big(-36k^3\pi^2 r_+\alpha^2(R-2\delta)\\ &+8P\pi r_+^4\big(2+\pi^2 r_+^3(-3R+4\delta)\big)+3kr_+^2\big(-2+\pi\\ &\big(32P\alpha+\pi r_+^3(-3R-32P\pi R\alpha+2\delta+64P\pi\alpha\delta)\big)\big)\\ &+16k\alpha\big(-1+\pi^2 r_+^3(3R-2\delta)\big)\phi^2+4r_+^2\big(2+\pi^2 r_+^3\\ &\times(3R-2\delta)\big)\phi^2-12k^2\alpha\big(-1+\pi^2 r_+\big(r_+^2(3R\\ &+8P\pi R\alpha-2\delta-32P\pi\alpha\delta)-4\alpha(R-2\delta)\phi^2\big)\big)\Big)^{-1}. \end{aligned} \tag{3.11}$$

Figure 2 illustrates the relationship between the heat capacity and the radius of the horizon with $\alpha = 0.01,\ 0.05,$ 0.5 and the variable value of the parameters. The trajectories are denoted in the red curve for $\alpha = 0.01$, the green curve for $\alpha = 0.05$, and the blue curve for $\alpha = 0.5$. The thermodynamic stability of the BH can be analyzed using specific heat, where positive values imply a stable state, while negative heat capacities suggest the system is thermodynamically unstable. In Fig. 2a, we get C_ϕ as the function of r_+ by inserting $\phi = 0.5,\ P = 0.01,\ \alpha = 0.01$ and $k = -1$. It shows that the behavior at lower values of r_+ is a thermodynamic instability due to negative specific heat. With increasing r_+, the positive value of the specific heat suggests a transition to a stable thermodynamic phase. Increasing the coupling constant α moves the transition point to higher values of r_+, suggesting that higher α improves the stability of the system at larger radii. The system maintains stable thermodynamic behavior as the specific heat remains positive. In Fig. 2b, we obtain C_ϕ as the function of r_+ by inserting $\phi = 0.5,\ P = 0.01,\ \alpha = 0.05$ and $k = 0$. The specific heat increases gradually with the radius of the horizon r_+, suggesting that the thermodynamic behavior is more stable throughout the region. In the early region, for smaller values of r_+, the specific location of the transition point is affected by the value of α. The specific heat increases and remains positive. This indicates that BHs within these circumstances maintain stable thermodynamic behavior. However, stability is more uniformly stable in Fig. 2b. In Fig. 2c, C_ϕ as the function of r_+ by inserting $\phi = 0.5,\ P = 0.01,\ \alpha = 0.5$ and $k = 1$. In the early region of Fig. 2c, for smaller values of r_+, the heat capacity shows negative behavior, suggesting an unstable BH phase. When the horizon radius increases, the heat capacity becomes positive, marking a transition to a stable BH phase.

3.3 Gibbs free energy

The on-shell GFE serves as a crucial tool in investigating the global thermodynamic stability and phase behavior of BHs. The on-shell GFE is described in detail in the literature [77], and it can be defined as follows

$$G = M - \frac{S_{\rm SM}}{\tau} - \phi\, Q, \tag{3.12}$$

where τ is the inverse of the conjugate temperature corresponding to the Sharma–Mittal entropy. We compute the on-shell GFE to determine the global stability of the BH, by inserting Eqs. (3.1), (3.5), (3.8), (3.9) into Eq. (3.12), which can be written as

$$G = \frac{8-8\left(1+\frac{1}{2}\pi^2 r_+(r_+^2+6k\alpha)\delta\right)^{\frac{R}{\delta}}+\pi R\tau\left(3kr_+^2+4P\pi r_+^4+3k^2\alpha-4r_+^2\phi^2\right)}{8R\tau}. \tag{3.13}$$

Figure 3 show a graphical representation of GFE along with the horizon radius (r_+) for the fixed value of $\alpha = 0.01,\ 0.05,\ 0.5$. The red curve represents $\alpha = 0.01$, the green curve represents $\alpha = 0.05$, and the blue curve represents $\alpha = 0.5$. The behavior of GFE is graphically obtained by putting $\phi = 0.5$, $P = 0.01$, and $k = -1,\ 0,\ 1$ in Fig. 3a–c, respectively. Negative values of GFE indicate instability, positive values of GFE suggest stability, and zero corresponds to the occurrence of a phase transition. The graph 3a highlights the behavior of GFE as the horizon radius changes with the varying GB coupling constant α. In the early region, for smaller values of r_+, the specific location of the transition point is affected by the value of α. The figure also shows that with higher values of α, the stability transition occurs at larger values of r_+, indicating that increasing the coupling constant delays instability. Even at large horizon radii, the GFE becomes positive for all potential values, implying that larger BHs are thermodynamically stable. In the context of BHs, this suggests that the BH is in a state of thermodynamic stability. It can be seen that GFE is negative in the early region of the horizon radius. GFE describes BH global stability. The positive trajectories along the horizon radius for all values of α represent the stable region. In Fig. 3b, GFE is an initial decrease with negative behavior and is graphically obtained

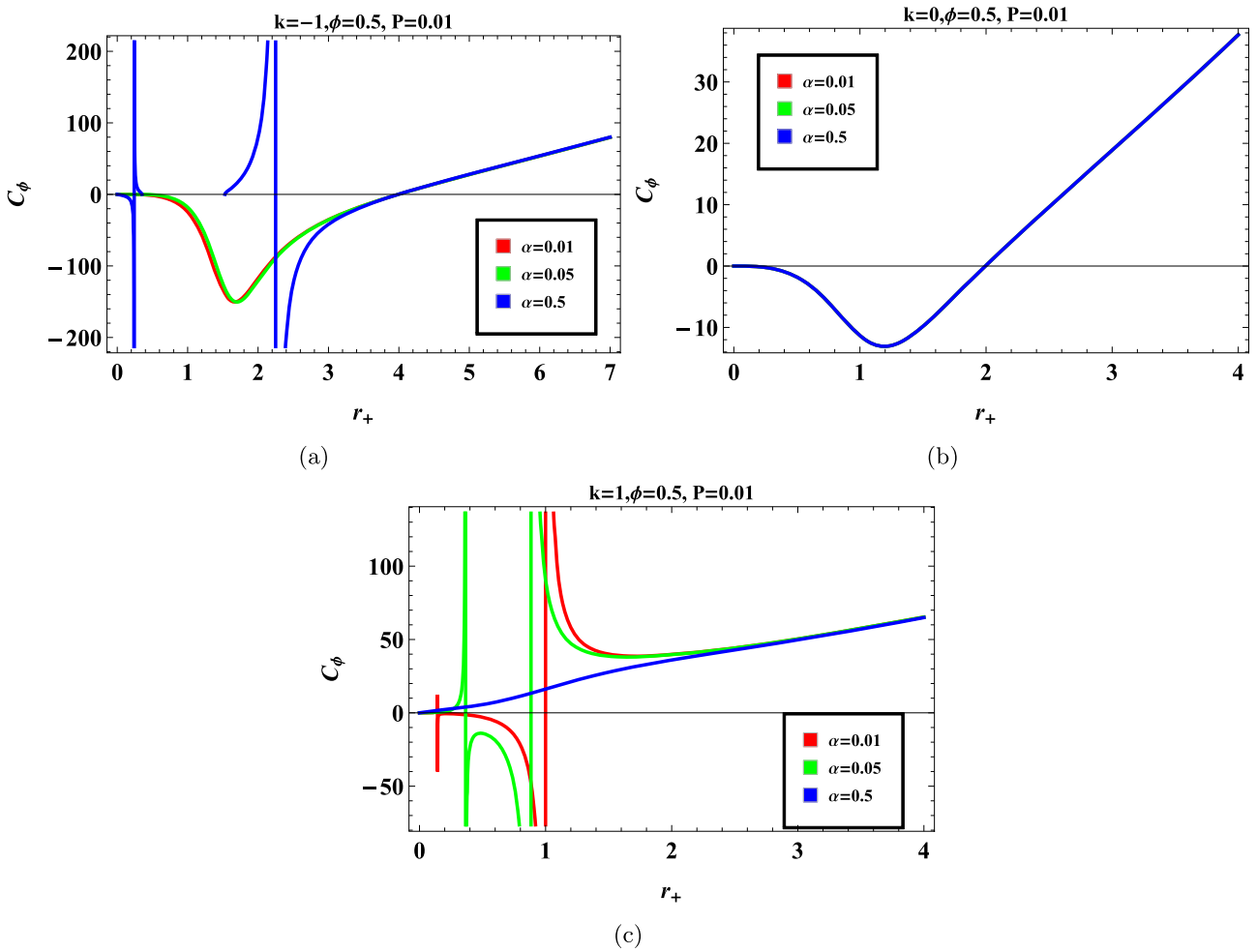

Fig. 2 Plots of specific heat versus horizon radius for BH solutions with $k = -1$ (**a**), $k = 0$ (**b**) and $k = 1$ (**c**). The red, green and blue curves correspond to three values of $\alpha = 0.01,\ 0.05,\ 0.5$, respectively

by putting $\phi = 0.5$, $P = 0.01$, and $k = 0$. It can be seen in Fig. 3c that the GFE is positive throughout the region. GFE describes BH global stability. The positive trajectories along the horizon radius for all values of α represent the stable region. The figure emphasizes the role of higher curvature, not effects, such as the GB term α, which influence the BH being stable.

4 Sparsity of Hawking radiations and emission of energy via Sharma–Mittal entropy

In this section, we discuss the sparsity of Hawking radiations and emission of energy for analyzing the Hawking radiations phenomenon in the presence of Sharma–Mittal entropy, respectively. Firstly, we explore the concept of BH sparsity, highlighting how BHs emit radiation similar to black bodies, with the temperature governed by their surface gravity. Hawking radiation differs significantly from classical black-body radiation, exhibiting an exceptionally sparse character as the BH evaporates. As defined in Refs. [57,78], sparsity measures the average interval between the emissions of adjacent quanta, which is determined by the energies associated with those emissions. It can be written as

$$\eta = \frac{C}{g}\left(\frac{\lambda_t^2}{\mathbb{A}_{eff}}\right), \tag{4.1}$$

where the thermal wavelength is defined as $\lambda_t = 2\pi/T$, $\tilde{g}$ characterizes the spin degeneracy of the emitted quanta, and the BH's effective area is $\mathbb{A}_{eff} = 27A_{BH}/4$. Here, C is defined as a parameter without any physical dimensions and for a simple Schwarzschild BH scenario with the emission of massless spin-1 bosons and $\lambda_t = 8\pi r_+^2$, the resulting efficiency is $\eta_{SH} \approx 64\pi^3/27 \approx 73.49$. Let us mention here that we use the conjugate temperature that corresponds to Sharma–Mittal entropy given in Eq. (3.3) to discuss the sparsity instead of the Hawking temperature. It is worth recalling

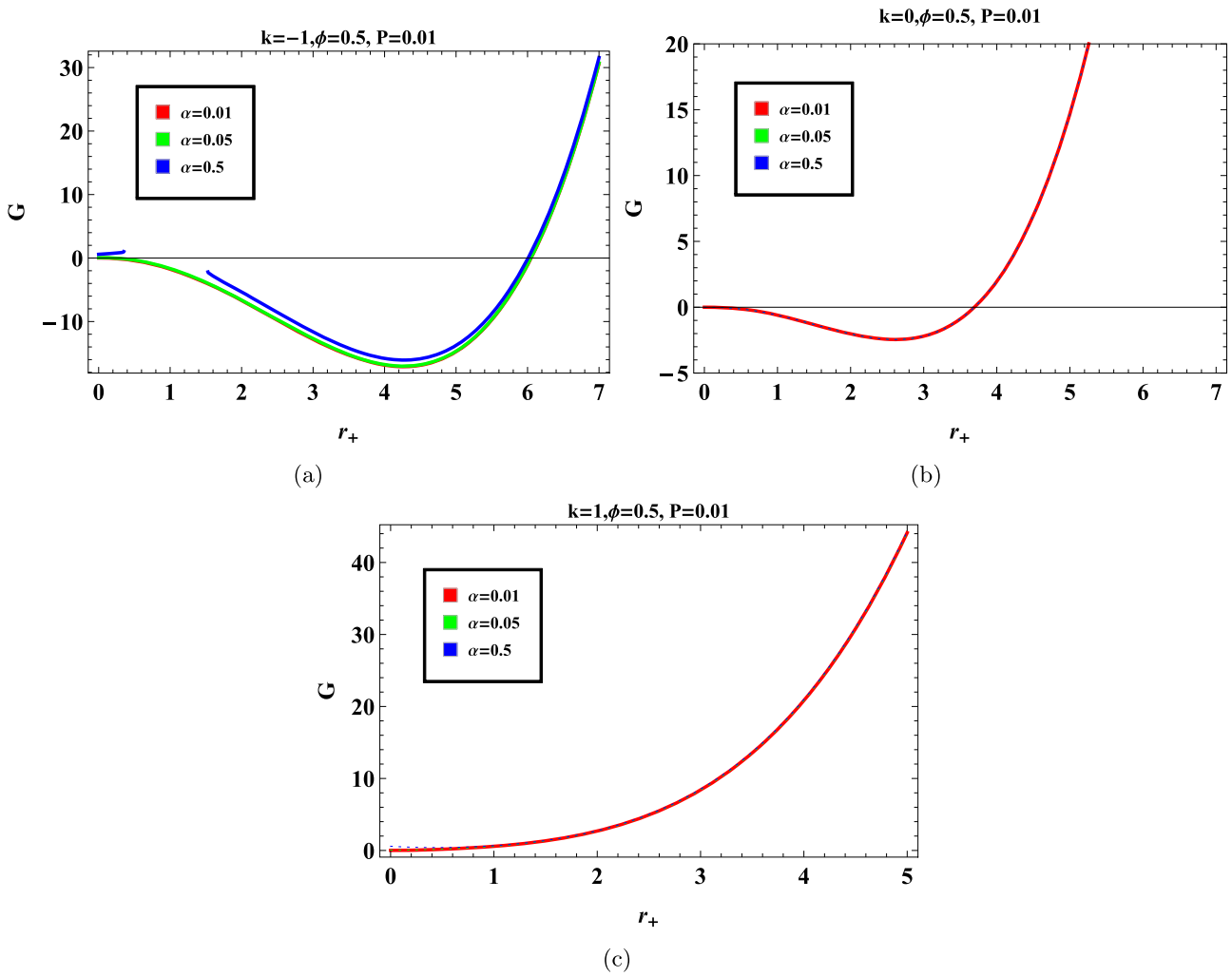

Fig. 3 Plots of GFE versus horizon radius for BH solutions with $k = -1$ (**a**), $k = 0$ (**b**) and $k = 1$ (**c**). The red, green and blue curves correspond to three values of $\alpha = 0.01,\ 0.05,\ 0.5$, respectively

that $\eta \ll 1$ in the case of black body radiation as a reference point.

$$\eta_{SM} = \frac{\pi^3\, C\, 2^{6-\frac{2R}{\delta}} \left(2\alpha k + r_+^2\right)^2 \left(\pi^2 \delta r_+ \left(6\alpha k + r_+^2\right) + 2\right)^{\frac{2R}{\delta}-2}}{3g r_+^4 \left(3k + 8\pi P r_+^2 - 4\phi^2\right)^2}. \tag{4.2}$$

To examine how changes in BH system parameters influence Hawking sparsity by using Sharma–Mittal entropy, Fig. 4 illustrates the variation of the specific quantity η with respect to Horizon radius r_+ for different values of k by putting $\phi = 0.5,\ P = 0.01,\ R = 0.1,\ \delta = 0.2$, for various trajectories we used $\alpha = 0.01$ (red curve), $\alpha = 0.05$ (green curve) and $\alpha = 0.5$ (blue curve). We insert the parameter $k = -1$ in Fig. 4a, $k = 0$ in Fig. 4b and $k = 1$ in Fig. 4c. Sparsity diminishes with increasing r_+, which differs from the behavior seen in Schwarzschild's BHs. At small values of r_+, the sparsity surpasses the standard Schwarzschild value η_{Sch}, meaning that the BH emits radiation that is sparser than Hawking radiation at this evaporation stage. When r_+ increases, η is consistently reduced and gets closer to zero in the limit. Notably, variations in the BH parameter space lead to significant variations in the decay trend. We see that in all cases of k, the behavior of all curves becomes convergent. In Fig. 4a, b with hyperbolic and planar geometry, they show slow behavior that goes to zero, but in Fig. 4c, for $k = 1$ (spherical geometry), even with small values of the Horizon radius, it becomes zero.

Hawking radiation causes the creation of particles and antiparticles, as well as the event horizon r_h. Additionally, evaporation starts when positively charged particles leave the central areas of Hawking radiation by means of quantum tunneling. The rate of energy release, which can be seen by an observer situated a considerable distance from the BH, determines the pace of BH evaporation. A large energy-absorption

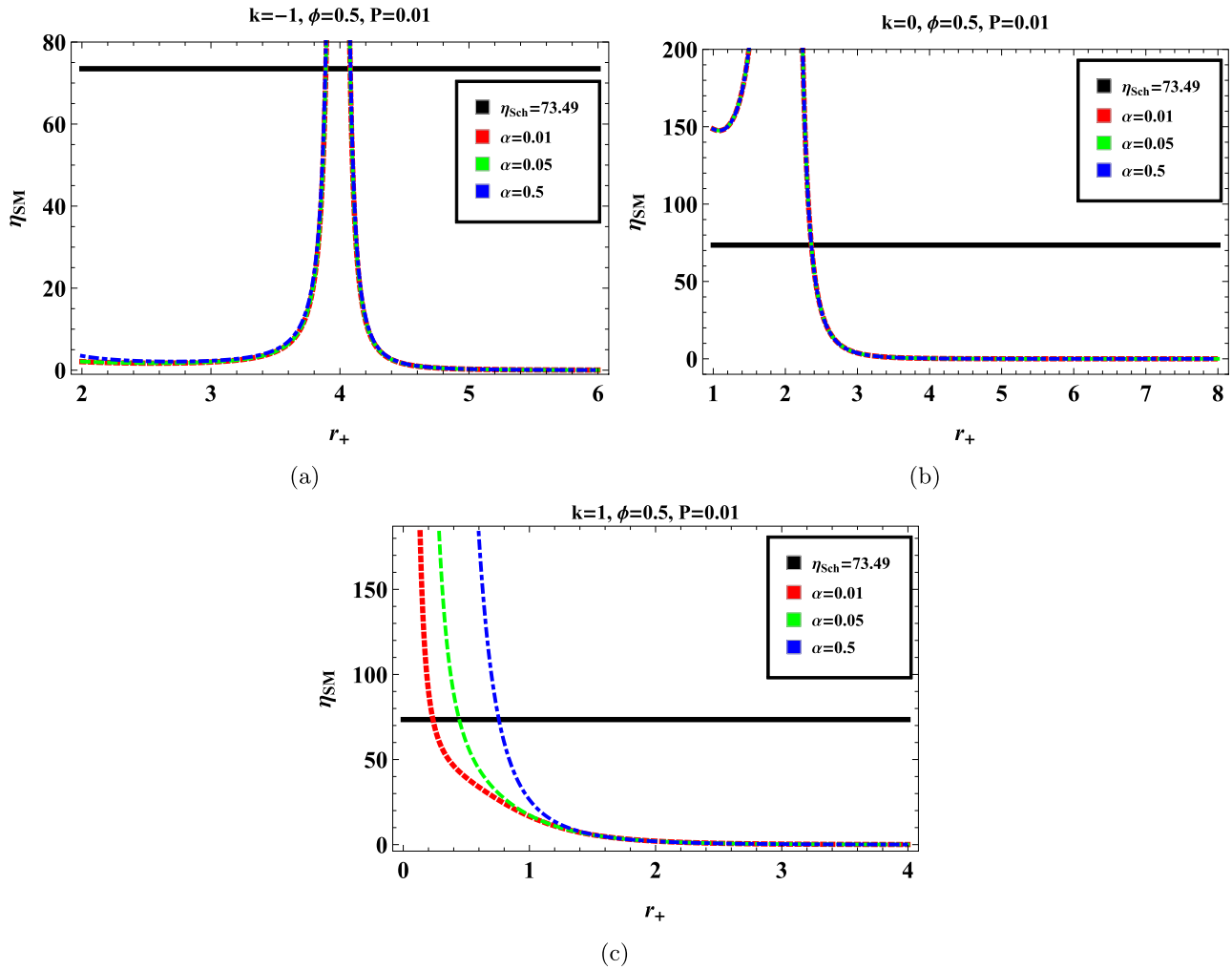

Fig. 4 Plots of emission of energy (η) versus horizon radius for BH solutions with $k=-1$ (**a**), $k=0$ (**b**) and $k=1$ (**c**). The red, green and blue curves correspond to three values of $\alpha=0.01,\ 0.05,\ 0.5$, respectively

cross section for this observer is connected with the BH shadow, which is an indication of the BH interaction with incoming radiation. The limiting value of the cross section corresponds to [79].

$$\sigma_{\rm lim}=\pi r_{+}^{2}. \tag{4.3}$$

Therefore, the rate of BH energy emission is given by

$$\frac{d^{2}\varepsilon}{{\rm d}\mu{\rm dt}}=\frac{2\pi^{2}r_{+}\mu^{3}}{e^{\mu/T}-1}. \tag{4.4}$$

In order to find the rate of BH energy emission, we use Eqs. (3.9) and (4.4), we get

$$\varepsilon_{\mu}=\frac{2\pi^{2}r_{+}\mu^{3}}{\exp\left(\frac{3\pi\mu\left(2\alpha k+r_{+}^{2}\right)}{r_{+}2^{\frac{R}{\delta}-2}\left(3k+8\pi Pr_{+}^{2}-4\phi^{2}\right)\left(\pi^{2}\delta r_{+}\left(6\alpha k+r_{+}^{2}\right)+2\right)^{1-\frac{R}{\delta}}}\right)-1}, \tag{4.5}$$

The plot of emission energy rate ($\varepsilon_{\mu t}$) versus horizon radius is shown in Fig. 5 by assuming the same constant parameters. For BH solutions corresponding to values $k=-1,\ 0$, the emission energy rate shows a constant behavior for smaller horizon radius, whereas an increasing behavior for larger BH. This depicts the emission of radiation faster for larger BHs. For the BH solution with $k=+1$, the energy emission shows fluctuations (initially it shows an increasing behavior, then attains a specific peak, and then shows a decreasing behavior) for a smaller radius, whereas it exhibits an increasing behavior for the case $\alpha=0.01$. This shows a complex behavior of BH evaporation, but for the larger BH (with a larger horizon radius), the BH radiates forever. For other choices of α, this BH solution represents a similar behavior as mentioned for the cases $k=-1,\ 0$. It became more difficult to identify BH in high-energy configurations as a result of changes in the emission spectra, which caused it to produce low-frequency radiation with a large entropy. In the context of astronom-

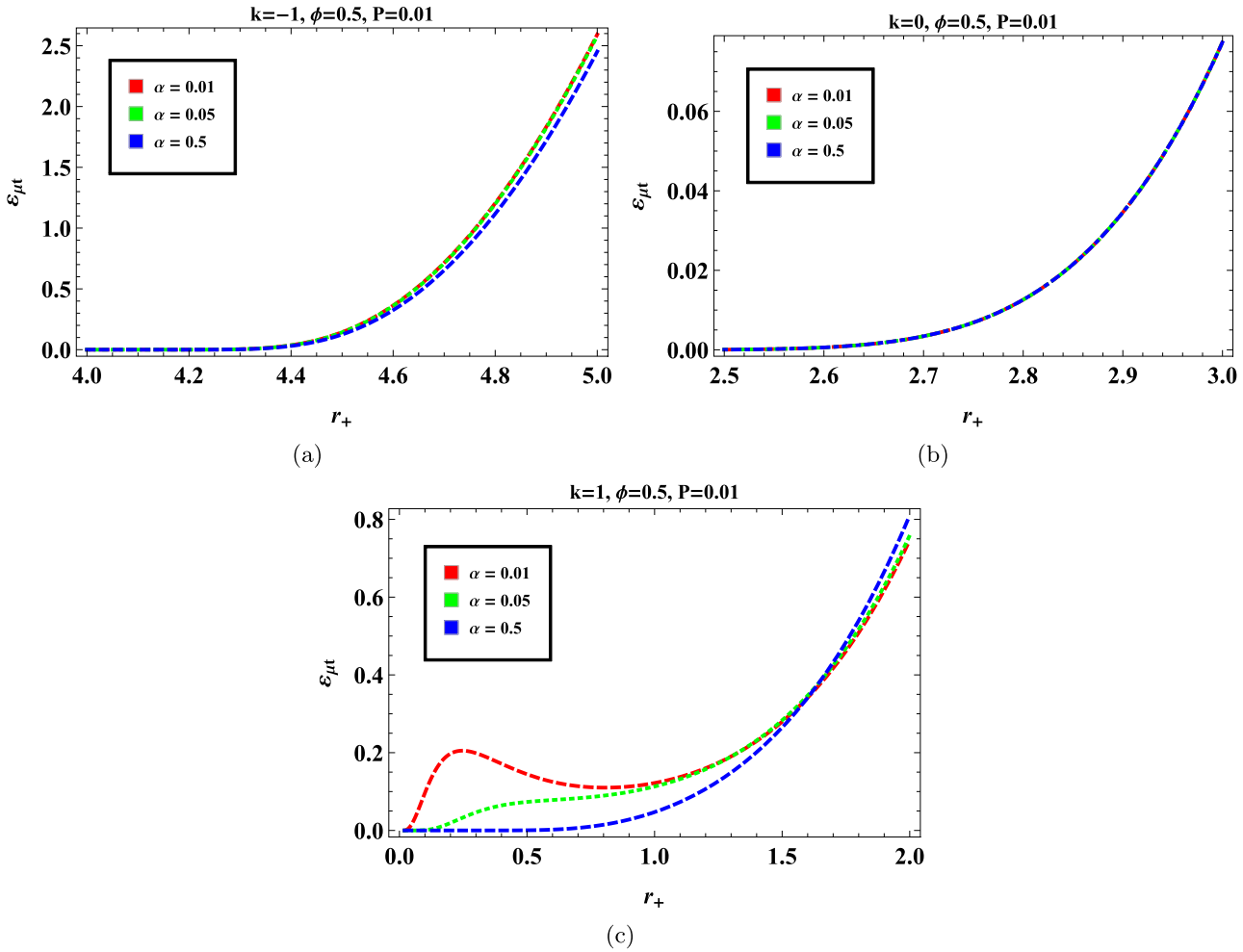

Fig. 5 Plots of emission of energy ($\varepsilon_{\mu t}$) versus horizon radius for BH solutions with $k = -1$ (**a**), $k = 0$ (**b**) and $k = 1$ (**c**). The red, green and blue curves correspond to three values of $\alpha = 0.01,\ 0.05,\ 0.5$, respectively

ical observations of BHs evaporating, the impacts of these actions play a significant role in differentiating between various gravity principles and standard GR.

5 Thermodynamical topology of black holes via Sharma–Mittal entropy

In this section, we basically describe the basic framework of the thermodynamic topology in which Duan's current mapping theory is used to determine the non-zero topological charge. Examining the topological properties of BH thermodynamics highlights the relationship between thermodynamic behavior and the topological framework of BHs [80]. Topological thermodynamics applies thermodynamic concepts with topological approaches to analyze structural properties, especially in the context of phase transitions and critical behavior. This framework examines topological invariants, including winding numbers, to explore thermodynamic state spaces. BH physics uses topological thermodynamics to explore the stability and phase transition of BHs, associating thermodynamic quantities like entropy and temperature with the topological nature of spacetime. Additionally, we discuss the role of winding number (or topological charge) obtained by using Duan's current mapping theory in thermodynamic topology and its correspondence to the BH's stability. In thermodynamic space, a winding number describes how many times the rotation made by a vector field (which is generally the gradients of GFE or the temperature) near a critical point, often plotted in the (r_+, θ) plane [42]. A positive winding number 1 illustrates a stable thermodynamic configuration (novel phase), while the negative -1 indicates an unstable thermodynamic configuration (conventional configuration), and if we have topological charge or winding number 0, then it indicates the absence of any critical point. Furthermore, these integer values provide a topological invariant that classifies the BH stability independent of coordinate choices or particular parameterizations. Additionally, this classification

aligns with some known results: for example, Schwarzschild BH exhibits a total topological charge -1, RN BH yields a total topological charge 0, and RN-AdS BH has a topological charge $+1$ as described in Ref. [43,47]. These topological charges represent basic models in BH thermodynamics, offering a basis to compare with generalized solutions such as those found in EGBG using Sharma–Mittal entropy. Thereby, winding numbers provide a coordinate-independent approach for distinguishing between stable and unstable configurations, even in cases when analytic expressions are very intricate and complex due to curvature corrections or modified entropy models.

For higher-dimensional BHs or GBG, topological factors play a key role in determining thermodynamic stability and behavior across phase transitions [42]. To analyze the topological charges and classifications of BHs, we can apply both temperature and free energy methods as described in [9,10,42,43,46,47,81]. We now outline a generalized framework for discussing thermodynamic topology by introducing a general thermodynamic potential φ, which we replaced by inserting temperature and generalized on-shell GFE. Thus, we define the vector field for the generalized vector field potential φ, which is written as

$$\varphi = \left(\varphi^{r_+}, \varphi^{\theta}\right) = \left(\frac{\partial \varphi}{\partial r_+}, -\cot\theta \csc\theta\right). \tag{5.1}$$

Here, φ^{θ} approaches infinity, directed away from the origin at both $\theta = 0$ and $\theta = \pi$. The variable r_+ is defined over the interval $[0, \infty]$, and θ lies within the range $[0, \pi]$. According to Duan's ϕ_e-mapping theory, one can define a topological current

$$j^{\nu} = \frac{1}{2\pi}\varepsilon^{\nu\mu\rho}\varepsilon_{ab}\partial_{\mu}n^{\mathfrak{a}}\partial_{\rho}n^{\mathfrak{b}}, \tag{5.2}$$

where $\nu,\ \rho,\ \mu = 0, 1, 2$, and normalized vector fields are represented as $n^{\mathfrak{a}}$. Moreover, this normalized vector field is equal to $\left(n^1 = \frac{\varphi^{r_+}}{|\varphi|},\ n^2 = \frac{\varphi^{\theta}}{|\varphi|}\right)$. Moreover, the current conservation is given by [42]

$$j^{\nu};_{\nu} = 0. \tag{5.3}$$

By utilizing Eq. (5.3), one can determine the following form of j^{ν} is given as

$$j^{\nu} = \delta^2(\varphi) J^{\nu}\left(\frac{\varphi}{\mathfrak{y}}\right). \tag{5.4}$$

Here, the Jacobi tensor is defined in the following manner

$$\varepsilon^{ab} J^{\nu}\left(\frac{\varphi}{\mathfrak{y}}\right) = \varepsilon^{\nu\mu\rho}\partial_{\mu}\varphi^{\mathfrak{a}}\partial_{\rho}\varphi^{\mathfrak{b}}. \tag{5.5}$$

If we take $\nu = 0$, the calculation of $j^0\left(\frac{\varphi}{\mathfrak{y}}\right)$ becomes simplies to the form $\frac{\partial(\varphi^1,\varphi^2)}{\partial(\mathfrak{y}^1,\mathfrak{y}^2)}$. Hence, the topological charge W is determined as follows

$$W = \int_{\Sigma} j^0 d^2\mathfrak{y} = \sum_{i=1}^{n}\beta_i\eta_i = \sum_{i=1}^{n}\omega_i. \tag{5.6}$$

The term β_i here denotes the positive Hopf index, and η_i is defined by the requirement that $\text{sign}(j^0(\varphi/\mathfrak{y})_{z_i})$ be equal to $+1,\ -1$. The sign of the winding number is essential for evaluating BH stability: a positive sign reflects a stable condition, while a negative sign reveals an unstable one.

The winding number represents a mathematical tool in topology to measure how a vector field or curve rotates around a certain point or any specific area. The winding number is utilized to analyze the phase transitions and BH stability by examining how a vector field behaves within a particular thermodynamic plane, as observed in the $r_+ - \theta$ plane. A nonzero winding number identifies a phase in which a BH maintains stability and does not undergo a transition shift to another phase due to slight perturbations in pressure and temperature. Modifications in the winding number indicate the presence of phase transitions, highlighting shifts during which BHs undergo a transition between stable configurations. In the context of an extended phase space, this framework is especially useful in analyzing the critical thermodynamic behavior of BHs. Now, we employed this framework to this BH solution in terms of the Sharma–Mittal entropy by using the temperature given in Eq. (3.1) and On-shell GFE given in Eq. (3.13).

For a thermodynamic system, we can evaluate its topological charge by designating $\sum$ as the full thermodynamic phase space. Different thermodynamic systems can be classified into distinct categories. This facilitates the analysis of topological transitions among various thermodynamic systems. Recent studies [26] have established that every critical point associated with a topological charge can be separated into two main categories: conventional (with $\omega_i = -1$) and novel (with $\omega_i = +1$). Q_t can be negative or positive at critical points when the winding number can be -1 or $+1$.

5.1 Temperature method

Duan's Potential acts as a fundamental model applied to explore topological properties within various physical systems. Duan's potential is recognized as a topological invariant originating from field configurations, enabling the categorization of topological charges based on winding numbers or other relevant invariants. In the context of BH theory, this framework has been applied to analyze the topological characteristics of spacetime, providing a deeper understanding of the global structure of BH solutions. The Duan potential establishes a comprehensive framework that associates topological effects with physical observables, which is especially valuable in the context of higher-dimensional or altered

gravity theories. In the investigation of BH phase transitions in GBG, Duan's topological current theory has been used to describe transitions as interchanges of winding number defects, providing a topological approach to the thermodynamics of BHs [82]. By the definition of Duan's potential

$$\varphi = \frac{1}{Sin\theta} T\left(r_+, z^i\right). \tag{5.7}$$

$$\times(3R-2\delta)\Big)\Big(1+\frac{1}{2}\pi^2 r_+\left(r_+^2+6k\alpha\right)\delta\Big)^{1-\frac{R}{\delta}}(3k-4\phi^2)\Big)$$
$$\times\Big(3\pi\big(-2r_+^2-12k\alpha+12k^2\pi^2 r_+\alpha^2\left(R-4\delta\right)$$
$$\times+\pi^2 r_+^5\left(3R-4\delta\right)+12k\pi^2 r_+^3\alpha\left(R-2\delta\right)\big)^2\Big)^{-1}, \tag{5.10}$$

$$\varphi^\theta = \left(\frac{\partial\varphi}{\partial\theta}\right)_{\phi,r_+} = -\frac{2^{-1+\frac{R}{\delta}} r_+\left(2+\pi^2 r_+\left(r_+^2+6k\alpha\right)\delta\right)^{2-\frac{R}{\delta}}\left(3k-4\phi^2\right)\cot\theta\csc\theta}{3\pi\left(2r_+^2+12k\alpha-12k^2\pi^2 r_+\alpha^2\left(R-4\delta\right)-12k\pi^2 r_+^3\alpha\left(R-2\delta\right)+\pi^2 r_+^5\left(-3R+4\delta\right)\right)}. \tag{5.11}$$

This expression defines the thermodynamic potential calculated on the basis of BH temperature. In this context, r_+ corresponds to the radius of the horizon and z^i indicates other parameters such as pressure and charge. The presence of $\frac{1}{sin\theta}$ promotes the investigation in the thermodynamic system, especially in topological investigations. In order to discuss the thermodynamic topology using the temperature given in Eq. (3.9), we eliminate the thermodynamic pressure as described in Ref. [81]. Equation (5.8) gives a representation of the pressure in terms of the thermodynamic parameters and the BH's horizon radius. Applying this condition $\left(\frac{\partial T}{\partial r_+}\right)_{P,\phi} = 0$, we get

$$P = -\frac{\Big(2r_+^2-4k\alpha+12k^2\pi^2 r_+\alpha^2\left(R-2\delta\right)+\pi^2 r_+^5\left(3R-2\delta\right)+4k\pi^2 r_+^3\alpha\left(3R-2\delta\right)\Big)\left(3k-4\phi^2\right)}{8\pi r_+^2\left(-2r_+^2-12k\alpha+12k^2\pi^2 r_+\alpha^2\left(R-4\delta\right)+\pi^2 r_+^5\left(3R-4\delta\right)+12k\pi^2 r_+^3\alpha(R-2\delta)\right)}. \tag{5.8}$$

By employing Eqs. (3.1) and (5.8), one can define the thermodynamic potential for the temperature method, which plays a crucial role in how the phase structure of BHs changes, as it defines the circumstances for phase transitions and stability.

$$\varphi = \frac{2^{-1+\frac{R}{\delta}} r_+\left(2+\pi^2 r_+\left(r_+^2+6k\alpha\right)\delta\right)^{2-\frac{R}{\delta}}\left(3k-4\phi^2\right)\csc\ \theta}{3\pi\left(2r_+^2+12k\alpha-12k^2\pi^2 r_+\alpha^2\left(R-4\delta\right)-12k\pi^2 r_+^3\alpha\left(R-2\delta\right)+\pi^2 r_+^5\left(-3R+4\delta\right)\right)}. \tag{5.9}$$

Now vector field $\varphi = \left(\varphi^{r_+}, \varphi^\theta\right)$ are formulated vector components as follows

$$\varphi^{r_+} = \left(\frac{\partial\varphi}{\partial r_+}\right)_{\phi,\theta} = \csc\theta\Big(\big(24k\alpha+r_+^2\left(-4+72k^3\pi^4\alpha^3\right.$$
$$\times(R-4\delta)(R-2\delta)\big)+2\pi^2 r_+^5\left(9R-11\delta\right)-72k^2\pi^2$$
$$\times r_+\alpha^2\left(R-3\delta\right)+36k^2\pi^4 r_+^4\alpha^2\left(3R-4\delta\right)\left(R-2\delta\right)$$
$$+\pi^4 r_+^8\left(3R-4\delta\right)\left(3R-2\delta\right)+6k\pi^4 r^6\alpha\left(3R-4\delta\right)$$

In order to obtain the topological charge, we utilize Eq. 5.6 as well as the normalized vector components n^1 and n^2 can be obtained through Eqs. (5.10) and (5.11). The normalized vector $n = \left(\frac{\varphi^{r+}}{||\varphi^+||}, \frac{\varphi^\theta}{||\varphi^\theta||}\right)$ is shown in Figs. 6a and 7. We know that if a critical point is enclosed by a closed contour, it will give us a topological charge of nonzero; otherwise, the topological charge is zero. For the purpose of evaluating the topological charge. In the following, we will define two contours, C_1 and C_2. They are described with parametrized by $\vartheta(\mathrm{v}) \in (0, 2\pi)$ $\{r = r_0 + x\cos v,\ \theta = \frac{\pi}{2} + y\sin v$. We use this formula to find the winding number or topological charge $d\Omega = \varepsilon_{ab} n^a dn^b = n^1 dn^2 - n^2 dn^1$ which are given in [83,84]. Hence, the topological charge can be expressed as $Q = \pm\frac{\Delta\Omega}{2\pi}$. In Fig. 6a, we have fixed $\alpha = 0.05$, $\phi = 0.5$, and $k = -1, 0, 1$, respectively. The blue arrows represent the vector field in the $r_+ - \theta$ plane. The black contours C_1 and C_2 in Fig. 6a, b are closed loops that include zero points that are conventional critical points. For the contour C_1, we clearly see that there is a phase transition of first order. In Fig. 6a, we have a critical point CP_1 which is enclosed by C_1 and the winding number corresponds to CP_1 is -1. Moreover, in Fig. 6b their exits only one single critical point CP_2. We encircle the critical point CP_2 by C_2 and the corresponding winding number or topological charge is -1.

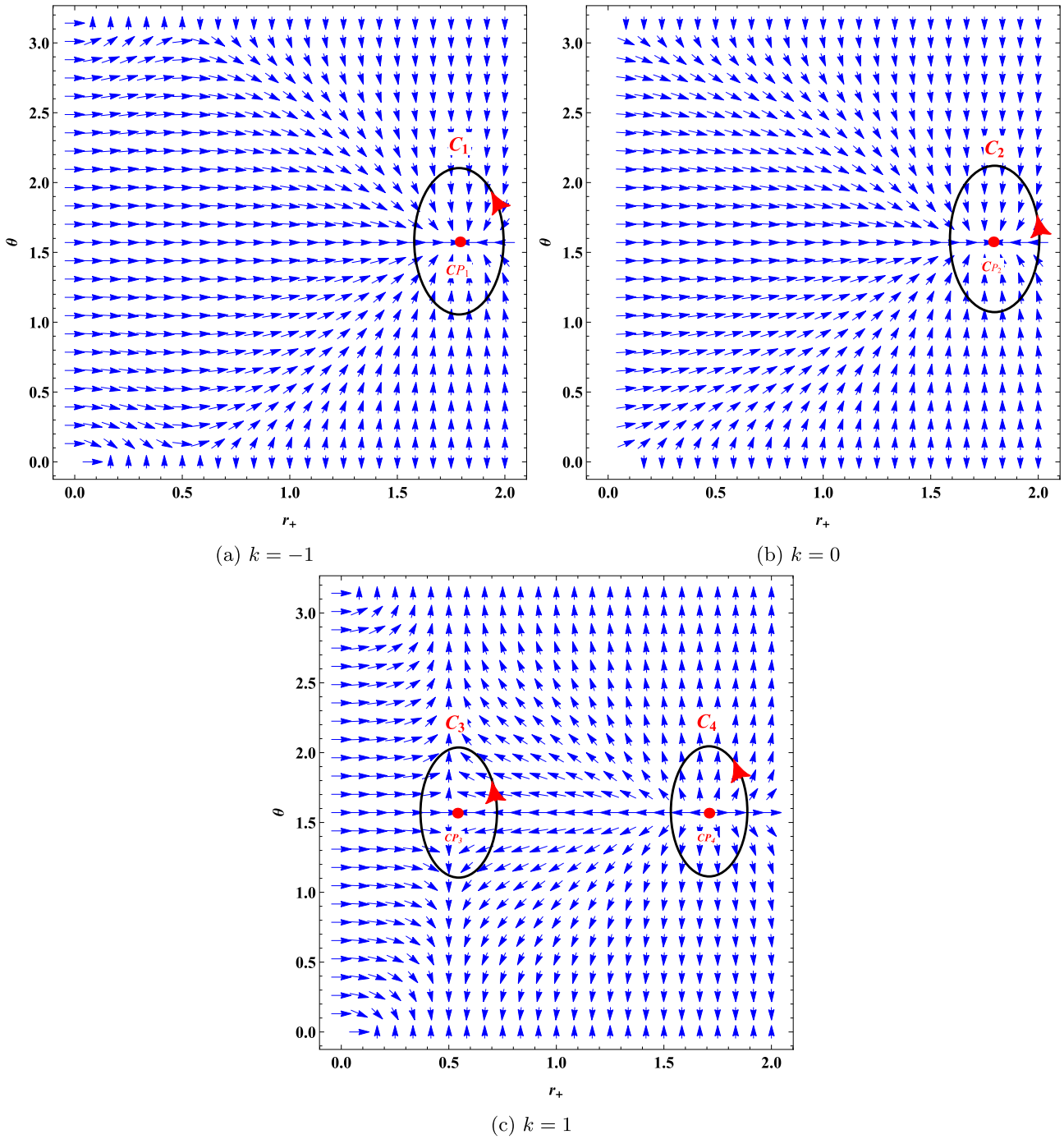

(a) $k = -1$ (b) $k = 0$

(c) $k = 1$

Fig. 6 Normalized vector field is plotted in $r_+ - \theta$ plane with $\alpha = 0.05$ and $\phi = 0.5$. The zero points are marked with red dot CP_1, CP_2, CP_3, and CP_4 and located at $(r_+, \theta) = (1.794, \frac{\pi}{2})$, $(1.794, \frac{\pi}{2})$, $(0.5463, \frac{\pi}{2})$, and $(1.704, \frac{\pi}{2})$ respectively. **a** $k = -1$, **b** $k = 0$, and **c** $k = 1$

In Fig. 6c, we found two critical points CP_3 (conventional) and CP_4 (novel) which are enclosed by C_3 and C_4 for the case of $k = 1$. They yield distinct topological charges; $\omega_{CP_3} = -1$ and $\omega_{CP_4} = +1$. Due to their distinct values, these two critical points are assigned separate topological classes. In this scenario, the total topological charge (TTC) is zero. To summarize the results, we give details in Table 1.

5.2 Generalized free energy method

GFE is an essential thermodynamic factor that establishes the phase behavior and stability of BHs. The behavior of GFE offers valuable information about phase transitions, where a change in its value highlights a shift between the BH behavior of stable and unstable phases. A vector field φ is defined from

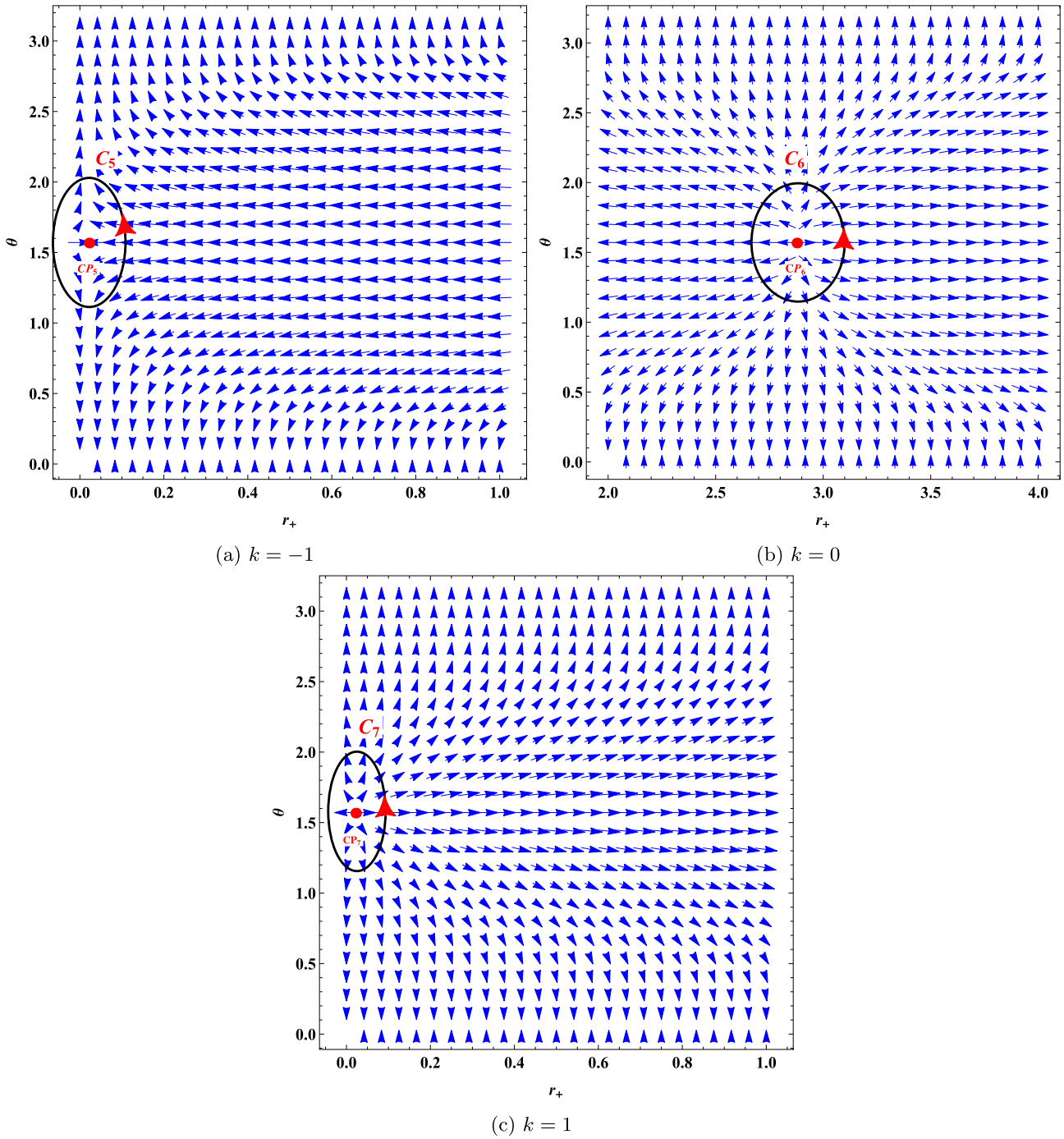

(a) $k = -1$ (b) $k = 0$

(c) $k = 1$

Fig. 7 Normalized vector field is plotted in $r_+ - \theta$ plane with $\alpha = 0.05$, $\phi = 0.5$, and $k = -1,\ 0,\ 1$. The zero points are marked with red dot CP_5, CP_6, and CP_7 and located at $(r_+, \theta) = (0.0455, \frac{\pi}{2})$, $(2.878, \frac{\pi}{2})$, and $(0.0509, \frac{\pi}{2})$

G given in Eq. (3.13), which takes the following shape

$$\varphi = \left(\frac{\partial G}{\partial r_+}, -\cot\theta \csc\theta\right), \tag{5.12}$$

And, we compute the vector components, which yield

$$\varphi^{r_+} = \frac{\partial G}{\partial r_+}, \quad \varphi^{\theta} = -\cot\theta \csc\theta, \tag{5.13}$$

Table 1 Summary of topological charges obtained in T-method using the Sharma–Mittal entropy for the BHs solution in EGBG and its comparison with different values of k. Here, we present critical points, winding number topological charge, and total topological charge by CPs, ω, and TTC, respectively

Case	CPs	ω	TTC
$k=-1$	1	$CP_1=-1$	-1
$k=0$	1	$CP_2=-1$	-1
$k=1$	2	$CP_3=-1, CP_4=+1$	0

Table 2 Summary of topological charges obtained in the free energy method using the Sharma–Mittal entropy for the BH solution in EGBG and its comparison with different values of k. Here, we present critical points, winding number topological charge, and total topological charge by CPs, ω, and TTC, respectively

Case	CP_s	ω	TTC
$k=-1$	1	$CP_5=-1$	-1
$k=0$	1	$CP_6=+1$	1
$k=1$	1	$CP_7=+1$	1

$$\varphi^{r_+}=\frac{\pi\Big(-3\times 2^{2-\frac{R}{\delta}}\pi\left(r_+^2+2k\alpha\right)\left(2+\pi^2 r_+\left(r_+^2+6k\alpha\right)\delta\right)^{-1+\frac{R}{\delta}}+r_+\tau\left(3k+8P\pi r_+^2-4\phi^2\right)\Big)}{4\tau}, \tag{5.14}$$

The corresponding unit vectors (n^1, n^2) are obtained as

$$n^1=\frac{\varphi^{r_+}}{\sqrt{\left(\varphi^{\theta}\right)^2+\left(\varphi^{r_+}\right)^2}},\quad n^2=\frac{\varphi^{\theta}}{\sqrt{\left(\varphi^{\theta}\right)^2+\left(\varphi^{r_+}\right)^2}} \tag{5.15}$$

$$n^1=\frac{\pi\Big(-3\times 2^{2-\frac{R}{\delta}}\pi\left(r_+^2+2k\alpha\right)\left(2+\pi^2 r_+\left(r_+^2+6k\alpha\right)\delta\right)^{-1+\frac{R}{\delta}}+r_+\tau\left(3k+8P\pi r_+^2-4\phi^2\right)\Big)}{4\tau\sqrt{\cot^2\theta\csc^2\theta+\frac{\pi^2\left(-3\times 2^{2-\frac{R}{\delta}}\pi\left(r_+^2+2k\alpha\right)\left(2+\pi^2 r_+\left(r_+^2+6k\alpha\right)\delta\right)^{-1+\frac{R}{\delta}}+r_+\tau\left(3k+8P\pi r_+^2-4\phi^2\right)\right)^2}{16\tau^2}}}, \tag{5.16}$$

$$n^2=-\frac{\cot\theta\csc\theta}{\sqrt{\cot^2\theta\csc^2\theta+\frac{\pi^2\left(-3\times 2^{2-\frac{R}{\delta}}\pi\left(r_+^2+2k\alpha\right)\left(2+\pi^2 r_+\left(r_+^2+6k\alpha\right)\delta\right)^{-1+\frac{R}{\delta}}+r_+\tau\left(3k+8P\pi r_+^2-4\phi^2\right)\right)^2}{16\tau^2}}}. \tag{5.17}$$

At the zero point $\varphi^{r_+}=0, \theta=\frac{\pi}{2}$, the relation for τ which is inverse of BH temperature ($\tau=\frac{1}{T}$) is expressed as

$$\tau=\frac{3\pi\left(r_+^2+2k\alpha\right)}{2^{-2+\frac{R}{\delta}}r_+\left(2+\pi^2 r_+\left(r_+^2+6k\alpha\right)\delta\right)^{1-\frac{R}{\delta}}\left(3k+8P\pi r_+^2-4\phi^2\right)}. \tag{5.18}$$

In Fig. 7, we have a critical point CP_5, CP_6, and CP_7 which are enclosed by contours C_5, C_6, and C_7. The winding numbers -1,+ 1 and + 1 are observed, respectively. Figure 7 shows the adjusted vector field plane $n^a=(n_1, n_2)$ in r_+ versus θ. In Fig. 7a CP_5, represented by the red dot, is a critical point for stability changes and phase transition. It is located at $(r_+, \theta)=(0.0455, \frac{\pi}{2})$. The vector illustrates the flow of thermodynamics, where CP_5 shows stability or instability through convergence or divergence. In Fig. 7a, we have a critical point and a topological charge TTC$=\omega_{CP_5}=-1$. In Fig. 7b CP_6, represented by the red dot, is a critical point for stability changes and phase transition. It is located at $(r_+, \theta)=(2.878, \frac{\pi}{2})$. We have a topological charge TTC$=\omega_{CP_6}=1$. For CP_7 enclosed by C_7 in Fig. 7c. CP_7 is a critical point located at $(r_+, \theta)=(0.0509, \frac{\pi}{2})$. Hence, the topological charge TTC is determined to be TTC$=\omega_{CP_7}=1$ 2.

6 Concluding remarks

In this work, we have explored the effects of the GB-corrected Sharma–Mittal entropy on the thermodynamics of five-dimensional BHs. In particular, we have investigated how BHs can undergo phase transitions, analogous to those in conventional thermodynamic systems, by examining their stability, entropy, and temperature profiles. These changes are governed by variables such as pressure, temperature, and other features that enhance our understanding of BH behavior in an advanced theoretical framework. This study provides a comprehensive evaluation of both the thermodynamics and topological characteristics of BHs. The intricate relationship between electric charge, mass, pressure, and entropy is extended by the first law of BH thermodynamics. In addition, the topological classification–obtained by Duan's potential theory and the GFE–reveals critical phase structures and elucidates the modifying characteristics of these BHs. In our analysis, we observed that the thermodynamic equilibrium conditions differentiate stable and unstable regimes and

impact phase transition behavior. Specifically, heat capacity C_ϕ played a crucial role in indicating the possible phase transition in these BHs. We observed that BHs exhibit from small to large phase transitions: for small horizon radii, the system is unstable, whereas stability emerges beyond a certain threshold. However, the GFE analysis generally indicates an overall unstable configuration. We determined the heat capacity and the GFE behavior for the cases of hyperbolic ($k = -1$), planar ($k = 0$), and spherical ($k = 1$), respectively.

Furthermore, Sharma–Mittal entropy generalizes the non-extensive thermodynamic phenomena more effectively than the traditional entropy models such as Bekenstein–Hawking, Tsallis and Rènyi entropies. As a result, the system shows more intricate behavior in terms of phase transition, stability, and topological charges. For example, in the case of Rènyi and exponential entropy obtained only limited topological charge as discussed in Refs. [62,67] but our analysis reveals both novel and conventional points depending on the horizon topology, Gauss–Bonnet coupling α, curvature parameter k and entropy parameters (R, δ). These distinctions reveal the unique and physically significant contribution of the Sharma–Mittal framework in capturing richer thermodynamics behavior of the higher-dimensional BHs in Gauss–Bonnet gravity. We have also determined the sparsity of Hawking radiation via the Sharma–Mittal entropy. As we mentioned in the earlier discussion of the behavior in Fig. 4, we examined the sparsity of Hawking radiation by using the conjugate temperature associated with the Sharma–Mittal entropy. We observed that initially, the sparsity parameter increases sharply for the small horizon radius, but as the horizon radius increases, the behavior of sparsity decreases, which finally converges to zero.

Furthermore, we have explored the thermodynamic topology for BHs with hyperbolic ($k = -1$), planar ($k = 0$), and spherical ($k = 1$) horizon geometries. We determined the normalized components and unit vectors of temperature and GFE and identified zero points in the relevant vector field plots presented in Figs. 6a and 7. These zero points reveal both conventional and novel critical points–conventional ones are typically linked with first-order transitions, which play a critical role in BH stability. In our study, we identified critical points characterized by winding numbers: $+1$ for stable cases and -1 for unstable ones. We further determined the topological charges for each horizon geometry ($k = -1, 0, 1$) and observed that the topological approach consistently distinguishes between stable ($+1$) and unstable (-1) phases. A negative total topological charge ($Q = -1$) corresponds to instability, while a positive charge ($Q = +1$) indicates stability. This analysis could be advanced in future work by examining how rotating or dynamical BHs in EGBG, framed within Sharma–Mittal entropy, impact thermodynamic stability and topological characteristics. The inclusion of quantum-level corrections may influence our understanding of microscopic thermodynamics, especially in the vicinity of critical points. In the future, we will extend this work and try to link these findings with observational features like BH shadows or gravitational wave echoes to investigate whether phase transitions or entropy corrections can be physically observed.

Acknowledgements This research is funded by the Science Committee of the Ministry of Science and Higher Education of the Republic of Kazakhstan (Grant no. AP23483654).

Data Availability Statement This manuscript has no associated data. [Author's' comment: Data sharing not applicable to this article as no datasets were generated or analysed during the current study.]

Code Availability Statement This manuscript has no associated code/software. [Author's comment: Code/Software sharing not applicable to this article as no code/software was generated or analysed during the current study.]

Funded by SCOAP[3].

References

1. R.V. Pound, G.A. Rebka Jr., Apparent weight of photons. Phys. Rev. Lett. **4**(7), 337 (1960)
2. A. Eckart, R. Genzel, Observations of stellar proper motions near the Galactic Centre. Nature **383**(6599), 415–417 (1996)
3. J.D. Bekenstein, Black holes and entropy. Phys. Rev. D **7**(8), 2333 (1973)
4. S.W. Hawking, Black hole explosions? Nature **248**(5443), 30–31 (1974)
5. R.M. Wald, The thermodynamics of black holes. Living Rev. Relativ. **4**, 1–44 (2001)
6. M. Sasada, Event Horizon Telescope Collaboration, First M87 event horizon telescope results. I. The shadow of the supermassive black hole. Astrophys. J. Lett. **875**(1), L1 (2019)
7. P.K. Yerra, C. Bhamidipati, Topology of black hole thermodynamics in Gauss-Bonnet gravity. Phys. Rev. D **105**(10), 104053 (2022)
8. S.J. Yang, M.S. Ali, S.W. Wei, Y.X. Liu, Holographic thermodynamics of a five-dimensional neutral Gauss–Bonnet AdS black hole. Eur. Phys. J. C **85**(4), 1–13 (2025)
9. S.W. Wei, Y.X. Liu, Extended thermodynamics and microstructures of four-dimensional charged Gauss–Bonnet black hole in AdS space. Phys. Rev. D **101**(10), 104018 (2020)
10. J. Sadeghi, M.A.S. Afshar, S.N. Gashti, M.R. Alipour, Thermodynamic topology of black holes from bulk-boundary, extended,

and restricted phase space perspectives. Ann. Phys. **460**, 169569 (2024)
11. S.W. Hawking, D.N. Page, Thermodynamics of black holes in anti-de Sitter space. Commun. Math. Phys. **87**, 577–588 (1983)
12. X.Y. Guo, H.F. Li, L.C. Zhang, R. Zhao, Microstructure and continuous phase transition of a Reissner–Nordstrom–AdS black hole. Phys. Rev. D **100**(6), 064036 (2019)
13. J. Maldacena, The large-N limit of superconformal field theories and supergravity. Int. J. Theor. Phys. **38**(4), 1113–1133 (1999)
14. S.S. Gubser, I.R. Klebanov, A.M. Polyakov, Gauge theory correlators from non-critical string theory. Phys. Lett. B **428**(1–2), 105–114 (1998)
15. A. Chamblin, R. Emparan, C.V. Johnson, R.C. Myers, Charged AdS black holes and catastrophic holography. Phys. Rev. D **60**(6), 064018 (1999)
16. A. Chamblin, R. Emparan, C.V. Johnson, R.C. Myers, Holography, thermodynamics, and fluctuations of charged AdS black holes. Phys. Rev. D **60**(10), 104026 (1999)
17. A. Karch, B. Robinson, Holographic black hole chemistry. J. High Energy Phys. **2015**(12), 1–15 (2015)
18. M.M. Caldarelli, G. Cognola, D. Klemm, Thermodynamics of Kerr–Newman–AdS black holes and conformal field theories. Class. Quantum Gravity **17**(2), 399 (2000)
19. D. Kastor, S. Ray, J. Traschen, Enthalpy and the mechanics of AdS black holes. Class. Quantum Gravity **26**(19), 195011 (2009)
20. M. Cvetič, G.W. Gibbons, D. Kubizňák, C.N. Pope, Black hole enthalpy and an entropy inequality for the thermodynamic volume. Phys. Rev. D Part. Fields Gravit. Cosmol. **84**(2), 024037 (2011)
21. B.P. Dolan, Pressure and volume in the first law of black hole thermodynamics. Class. Quantum Gravity **28**(23), 235017 (2011)
22. M. Appels, R. Gregory, D. Kubizňák, Thermodynamics of accelerating black holes. Phys. Rev. Lett. **117**(13), 131303 (2016)
23. M. Appels, R. Gregory, D. Kubizňák, Black hole thermodynamics with conical defects. J. High Energy Phys. **2017**(5), 1–24 (2017)
24. S. Gunasekaran, D. Kubizňák, R.B. Mann, Extended phase space thermodynamics for charged and rotating black holes and Born–Infeld vacuum polarization. J. High Energy Phys. **2012**(11), 1–43 (2012)
25. G.M. Deng, J. Fan, X. Li, Y.C. Huang, Thermodynamics and phase transition of charged AdS black holes with a global monopole. Int. J. Mod. Phys. A **33**(03), 1850022 (2018)
26. H. Abdusattar, Stability and Hawking-Page-like phase transition of phantom AdS black holes. Eur. Phys. J. C **83**(7), 614 (2023)
27. S.L. Li, H.D. Lyu, H.K. Deng, H. Wei, $P-V$ criticality in gauged supergravities. Eur. Phys. J. C Part. Fields **79**(3), 201 (2019)
28. S.H. Hendi, M.H. Vahidinia, Extended phase space thermodynamics and P-V criticality of black holes<? format?> with a nonlinear source. Phy. Rev. D Part. Fields Gravit. Cosmol. **88**(8), 084045 (2013)
29. J.X. Mo, W.B. Liu, Ehrenfest scheme for PV criticality in the extended phase space of black holes. Phys. Lett. B **727**(1–3), 336–339 (2013)
30. J. Xu, L.M. Cao, Y.P. Hu, P-V criticality in the extended phase space of black holes in massive gravity. Phys. Rev. D **91**(12), 124033 (2015)
31. D. Momeni, M. Faizal, K. Myrzakulov, R. Myrzakulov, Fidelity susceptibility as holographic PV-criticality. Phys. Lett. B **765**, 154–158 (2017)
32. S. Fernando, P-V criticality in AdS black holes of massive gravity. Phys. Rev. D **94**(12), 124049 (2016)
33. A. Kumar, S.G. Ghosh, A. Wang, Effect of dark energy on photon orbits and thermodynamic phase transition for Hayward anti-de Sitter black holes. Phys. Dark Universe **46**, 101608 (2024)
34. A. Sood, A. Kumar, J.K. Singh, S.G. Ghosh, Photon orbits and phase transitions in Kiselev–AdS black holes from f (R, T) gravity. Eur. Phys. J. C **84**(8), 876 (2024)
35. E. Elizalde, S.I. Nojiri, S.D. Odintsov, Black hole thermodynamics and generalised non-extensive entropy. Universe **11**(2), 60 (2025)
36. S.I. Nojiri, S.D. Odintsov, V. Faraoni, New entropies, black holes, and holographic dark energy. Astrophysics **65**(4), 534–551 (2022)
37. A.S. Jahromi, S.A. Moosavi, H. Moradpour, J.M. Graça, I.P. Lobo, I.G. Salako, A. Jawad, Generalized entropy formalism and a new holographic dark energy model. Phys. Lett. B **780**, 21–24 (2018)
38. C. Tsallis, Possible generalization of Boltzmann–Gibbs statistics. J. Stat. Phys. **52**, 479–487 (1988)
39. S.D. Odintsov, T. Paul, A non-singular generalized entropy and its implications on bounce cosmology. Phys. Dark Universe **39**, 101159 (2023)
40. N. Drepanou, A. Lymperis, E.N. Saridakis, K. Yesmakhanova, Kaniadakis holographic dark energy and cosmology. Eur. Phys. J. C **82**(5), 449 (2022)
41. Y.S. Myung, Y.W. Kim, Y.J. Park, Thermodynamics of Gauss–Bonnet black holes revisited. Eur. Phys. J. C **58**, 337–346 (2008)
42. S.W. Wei, Y.X. Liu, Topology of black hole thermodynamics. Phys. Rev. D **105**(10), 104003 (2022)
43. S.W. Wei, Y.X. Liu, R.B. Mann, Black hole solutions as topological thermodynamic defects. Phys. Rev. Lett. **129**(19), 191101 (2022)
44. N.C. Bai, L. Li, J. Tao, Topology of black hole thermodynamics in Lovelock gravity. Phys. Rev. D **107**(6), 064015 (2023)
45. P.K. Yerra, C. Bhamidipati, Topology of Born–Infeld AdS black holes in 4D novel Einstein–Gauss–Bonnet gravity. Phys. Lett. B **835**, 137591 (2022)
46. D. Wu, Topological classes of thermodynamics of the four-dimensional static accelerating black holes. Phys. Rev. D **108**(8), 084041 (2023)
47. D. Wu, S.Q. Wu, Topological classes of thermodynamics of rotating AdS black holes. Phys. Rev. D **107**(8), 084002 (2023)
48. W. Di, G. Shuang-Yong, Z. Xiao-Dan, J. Qing-Quan, Y. Shu-Zheng, Topological classes of thermodynamics of the static multi-charge AdS black holes in gauged supergravities: novel temperature-dependent thermodynamic topological phase transition. JHEP **6**, 213 (2024)
49. N.J. Gogoi, P. Phukon, Thermodynamic topology of 4D dyonic AdS black holes in different ensembles. Phys. Rev. D **108**(6), 066016 (2023)
50. C. Liu, J. Wang, Topological natures of the Gauss–Bonnet black hole in AdS space. Phys. Rev. D **107**(6), 064023 (2023)
51. M.R. Alipour, M.A.S. Afshar, S.N. Gashti, J. Sadeghi, Topological classification and black hole thermodynamics. Phys. Dark Universe **42**, 101361 (2023)
52. A. Kumar, A. Sood, S.G. Ghosh, A. Beesham, Hayward–Letelier Black Holes in AdS Spacetime. Particles **7**(4), 1017–1037 (2024)
53. M. Yasir, X. Tiecheng, A. Jawad, Topological charges via Barrow entropy of black hole in metric-affine gravity. Eur. Phys. J. C **84**(9), 1–15 (2024)
54. A. Kumar, S.G. Ghosh, A. Beesham, Extended phase space thermodynamics of Bardeen–Letelier black holes in 4D Einstein–Gauss–Bonnet gravity. Eur. Phys. J. Plus **139**(5), 439 (2024)
55. M.Y. Zhang, H. Chen, H. Hassanabadi, Z.W. Long, H. Yang, Thermodynamic topology of Kerr–Sen black holes via Renyi statistics. Phys. Lett. B **856**, 138885 (2024)
56. D.N. Page, Hawking radiation and black hole thermodynamics. New J. Phys. **7**(1), 203 (2005)
57. F. Gray, S. Schuster, A. Van-Brunt, M. Visser, The Hawking cascade from a black hole is extremely sparse. Class. Quantum Gravity **33**(11), 115003 (2016)
58. R.G. Cai, Gauss–Bonnet black holes in AdS spaces. Phys. Rev. D **65**(8), 084014 (2002)
59. S.W. Hawking, Particle creation by black holes. Commun. Math. Phys. **43**(3), 199–220 (1975)

60. S. Nojiri, S.D. Odintsov, V. Faraoni, How fundamental is entropy? From non-extensive statistics and black hole physics to the holographic dark universe. arXiv preprint arXiv:2201.02424
61. A. Rényi, On measures of entropy and information, in *Proceedings of the Fourth Berkeley Symposium on Mathematical Statistics and Probability, Volume 1: Contributions to the Theory of Statistics*, vol. 4 (University of California Press, 1961), pp. 547–562
62. S. Ghaffari, G.G. Luciano, A. Sheykhi, Nonextensive entropies impact onto thermodynamics and phase structure of Kerr–Newman black holes. Phys. Dark Universe **44**, 101447 (2024)
63. R. Horodecki, P. Horodecki, M. Horodecki, K. Horodecki, Quantum entanglement. Rev. Mod. Phys. **81**(2), 865–942 (2009)
64. S.D. Odintsov, T. Paul, Generalised (non-singular) entropy functions with applications to cosmology and black holes, in *International Conference on Frontiers of Fundamental Physics* (Springer International Publishing, Cham, 2022), pp. 165–192
65. A. Jawad, H. Tariq, S. Chaudhary, Q. Wu, Stability and thermodynamic geometry of black hole in generalized entropy framework. Ann. Phys. **473**, 169875 (2025)
66. H. Tariq, U. Zafar, S. Chaudhary, K. Bamba, A. Jawad, S. Shaymatov, Exploring the effects of generalized entropy onto Bardeen black hole surrounded by cloud of strings. Nucl. Phys. B **1016**, 116906 (2025)
67. S. Malik, A. Jawad, S. Chaudhary, M.M. Alam, S. Shaymatov, S. Rani, Thermodynamic aspects of higher-dimensional black holes in Einstein–Gauss–Bonnet gravity through exponential entropy. Commun. Theor. Phys. **77**(4), 045404 (2025)
68. H.M.M. Ahissou, I.G. Salako, A.V. Monwanou, A. Jawad, M.M. Alam, S. Shaymatov, H. Raza, Thermodynamics of f (T, T) gravity corrected black holes and physical consequences. Phys. Dark Universe **48**, 101850 (2025)
69. M. Masi, A step beyond Tsallis and Rényi entropies. Phys. Lett. A **338**(3–5), 217–224 (2005)
70. B.D. Sharma, D.P. Mittal, New non-additive measures of entropy for discrete probability distributions. J. Math. Sci. **10**(75), 28–40 (1975)
71. S.I. Nojiri, S.D. Odintsov, V. Faraoni, Alternative entropies and consistent black hole thermodynamics. Int. J. Geom. Methods Modern Phys. **19**(13), 2250210 (2022)
72. F. Nielsen, R. Nock, A closed-form expression for the Sharma–Mittal entropy of exponential families. J. Phys. A: Math. Theor. **45**(3), 032003 (2011)
73. E. Akturk, G.B. Bagci, R. Sever, Is Sharma–Mittal entropy really a step beyond Tsallis and Renyi entropies? (2007). arXiv preprint arXiv:cond-mat/0703277
74. M. Naeem, A. Bibi, Correction to the Friedmann equation with Sharma–Mittal entropy: a new perspective on cosmology. Ann. Phys. **462**, 169618 (2024)
75. T. Jacobson, Black hole thermodynamics today (1998). arXiv preprint arXiv:gr-qc/9801015
76. J.M. Bardeen, B. Carter, S.W. Hawking, The four laws of black hole mechanics. Commun. Math. Phys. **31**, 161–170 (1973)
77. I. Jeon, B.H. Lee, W. Lee, M. Mishra, Stability and topological nature of charged Gauss–Bonnet AdS black holes in five dimensions. Phys. Rev. D **111**(6), 064006 (2025)
78. D.N. Page, Particle emission rates from a black hole. II. Massless particles from a rotating hole. Phys. Rev. D **14**(12), 3260 (1976)
79. F. Mushtaq, A. Jawad, X. Tiecheng, M.M. Alam, S. Shaymatov, Probing deflection angle inspired by weak field of specific black holes in non plasma and plasma field. Phys. Dark Universe **48**, 101872 (2025)
80. Y. Sekhmani, S.N. Gashti, M.A.S. Afshar, M.R. Alipour, J. Sadeghi, J. Rayimbaev, Thermodynamic topology of Black Holes in $F(R)$-Euler–Heisenberg gravity's rainbow (2024). arXiv preprint arXiv:2409.04997
81. I. Jeon, B.H. Lee, W. Lee, M. Mishra, Stability and topological nature of charged Gauss–Bonnet AdS black holes in five dimensions (2024). arXiv preprint arXiv:2407.20016
82. C. Fairoos, Topological interpretation of black hole phase transition in Gauss–Bonnet gravity. Int. J. Mod. Phys. A **39**(05n06), 2450030 (2024)
83. S.W. Wei, Topological charge and black hole photon spheres. Phys. Rev. D **102**(6), 064039 (2020)
84. U. Zafar, K. Bamba, T. Rasheed, K. Bhattacharya, Thermodynamic analysis of black holes with cloud of strings and quintessence via Barrow entropy. Phys. Lett. B **864**, 139446 (2025)